DYNAMIC CONTRAST-ENHANCED MAGNETIC RESONANCE IMAGING OF CANINE BRAIN TUMORS

QUN ZHAO, SUNBOK LEE, MARC KENT, SCOTT SCHATZBERG, SIMON PLATT

We evaluated dynamic contrast-enhanced magnetic resonance imaging (DCE-MRI) in canine brain tumors. Magnetic resonance data sets were collected on seven canine intracranial tumors with a 3 T magnet using a T1-weighted fast spin echo fluid attenuated inversion recovery sequence after an IV bolus injection (0.2 mmol/kg) of Gd-DTPA. The tumors were confirmed histopathologically as adenocarcinoma ($n = 1$), ependymoma ($n = 1$), meningioma ($n = 3$), oligodendroglioma ($n = 1$), and pituitary macroadenoma ($n = 1$) The data were analyzed using a two-compartment pharmacokinetic model for estimation of three enhancement parameters, E_R (rate of enhancement), K_{el} (rate of elimination), and K_{ep} (rate constant), and a model-free phenomenologic parameter initial area under the Gd concentration curve (IAUGC) defined over the first 90 s postenhancement. Pearson's correlations were calculated between parameters of the two methods. The IAUGC has a relatively strong association with the rate of enhancement E_R, with r ranges from 0.4 to 0.9, but it was weakly associated with K_{ep} and K_{el}. To determine whether any two tumors differed significantly, the Kolmogorov–Smirnov test was used. The results showed that there were statistical differences ($P < 0.05$) between distributions of the enhancement pattern of each tumor. These kinetic parameters may characterize the perfusion and vascular permeability of the tumors and the IAUGC may reflect blood flow, vascular permeability, and the fraction of interstitial space. The kinetic parameters and the IAUGC derived from DCE-MRI present complementary information and they may be appropriate to noninvasively differentiate canine brain tumors although a larger prospective study is necessary. © 2010 *Veterinary Radiology & Ultrasound*

Key words: brain tumor, dynamic contrast-enhanced magnetic resonance imaging (DCE-MRI), pharmacokinetic modeling.

Introduction

THE COMMON CANINE brain tumors have gross, histologic, and molecular similarities to their human counterpart.[1–14] Thus, it is not surprising there are also many neuroimaging similarities.[15–17] Based on magnetic resonance (MR) imaging characteristics, a relatively specific diagnosis of some canine brain tumors can be rendered.[9–11,15–21] However, even in humans, the predictive accuracy of diagnosing specific tumor types with MR imaging varies between 65% and 96%.[22,23] MR features of canine brain tumors have not led to the identification of an association between imaging characteristics and tumor subtype, grade, and molecular composition.[15,24] Therefore, a definitive diagnosis of intracranial neoplasia requires histopathologic examination, but biopsy or resection of canine brain tumors is not always feasible. In such instances, the use of a noninvasive diagnostic imaging modality to more accurately predict tumor type and grade would be beneficial. Additionally, there is a need for early, noninvasive, functional, end points relating to tumor response in the assessment of novel anticancer therapies. Functional MR imaging techniques may be useful in these pursuits.

Lesion enhancement following IV contrast medium administration has led to improvement in the detection of primary brain tumors. However, contrast enhancement alone cannot be used to determine tumor type or identify objective parameters that can be used as markers of therapeutic effect in clinical trials. This is, in part, because contrast enhancement reflects a combination of the blood volume (vascularization), blood–brain barrier breakdown (microvessel permeability) and lesion interstitial space. Dynamic contrast-enhanced magnetic resonance imaging (DCE-MRI) is an imaging technique which can be used to investigate the physiology of tissue microvasculature and therefore serves as a more objective method of brain tumor assessment, both pre- and posttherapy than conventional MR imaging. For DCE-MRI, a series of MR images are acquired before, during, and after the injection of a paramagnetic contrast medium. Conventional MR imaging is basically an instantaneous representation of a structure at a given time, whereas DCE-MRI is a continuous evaluation

From the Department of Physics & Astronomy, BioImaging Research Center (Zhao, Lee) and the Department of Small Animal Medicine & Surgery (Kent, Schatzberg, Platt), University of Georgia, Athens, GA.

This study was supported by the faculty research grant (Zhao) from the University of Georgia.

Address correspondence and reprint requests to Qun Zhao, at the above address. E-mail: qzhao@physast.uga.edu

Received April 8, 2009; accepted for publication August 18, 2009.
doi: 10.1111/j.1740-8261.2009.01635.x

through a series of temporally sequential images. During the initial stage, the accumulation of contrast medium results in a signal increase on T1-weighted images that is usually described as a wash-in effect.[25] After the signal reaches a peak, it is followed by a signal decrease as the contrast medium is gradually eliminated from the tissue; this is described as a wash-out phenomenon. The graphical representation of signal intensity as a function of time after contrast medium administration is referred to as the signal enhancement curve.

Postprocessing and mathematic analysis of the sequential data produced by DCE-MRI can help determine tumor blood volume and vascular permeability.[26] These parameters are determined by tissue status, and they have been used in differentiating malignant from benign tumors,[25] determination of tumor staging,[27] and monitoring of tumor treatment response in humans.[28] DCE-MRI is therefore a promising noninvasive tool for many canine neurologic applications including cancer detection, diagnosis, staging, and assessment of treatment in addition to understanding the pathophysiology and behavior of brain tumors.

Analysis of DCE-MRI data has been based primarily on pharmacokinetic modeling, from which estimates of tissue perfusion and permeability can be derived, based on the contrast medium wash-in and wash-out curves.[29–32] A pharmacokinetic model refers to the model dealing with the process by which a drug is absorbed, distributed, metabolized, and eliminated by the body. The accuracy of DCE-MRI highly depends on pharmacokinetic modeling. Theoretic models, pharmacokinetic parameters, and the data collection procedures used, vary considerably in prior publications dealing with DCE-MRI in human tumors. Tofts and colleagues[29,30] proposed physiologic change-based parameters derived from a two-compartment model, given that the arterial input function can be measured or assumed. By measuring or estimating the physiologic parameters, theoretic values may be calculated for each tumor type and subsequently this information might allow for differentiation among brain tumor types. However, when the arterial input function is unavailable or difficult to measure, others have applied parameters to the pharmacokinetic models based on signal enhancement curve fitting,[31,33] without measuring/assuming the arterial input function. Another semiquantitative measure that is often used is the initial area under Gd concentration curve (IAUGC).[34] The IAUGC method was developed to provide a robust indicator of tumor vascular characteristics. This method does not attempt to estimate physiologic parameters related to tumor vasculature directly, but instead provides a measurement of the initial arrival of contrast medium in the tissue after its administration, which may reflect blood flow, vascular permeability, and the fraction of interstitial space.[29,30]

The aims of this study were to evaluate the use of DCE-MRI for canine brain tumors. More specifically, we aimed to assess pharmacokinetic differences between histopathologically diverse brain tumors that would subsequently allow for the development of a prospective study to more accurately assess the potential relevance DCE-MRI in predicting tumor type. Both quantitative pharmacokinetic modeling and model-free measurement of IAUGC were used and their correlation was also studied.

Materials and Methods

Data Acquisition

Seven dogs with an intracranial tumor were studied. All diagnostic investigations, including MR imaging, and tissue procurement procedures were performed as part of a routine clinical process with informed client consent. The dogs were premedicated with hydromorphone,* midazolam,† and glycopyrrolate.‡ Anesthesia was induced with propofol§ and maintained with isoflurane¶ and oxygen. Dogs were in sternal recumbency for imaging. After MR imaging, tissue obtained via craniectomy or at necropsy was examined histologically. The seven tumors were adenocarcinoma ($n = 1$), ependymoma ($n = 1$), meningioma ($n = 3$), oligodendroglioma ($n = 1$), and pituitary macroadenoma ($n = 1$).

Dogs were imaged using a 3 T HDx magnet‖ and a single-channel circular-polarized human knee coil. A T1-weighted fluid-attenuated inversion recovery (T1-weighted FLAIR) MR scan was used to acquire the DCE-MRI data in 2D transverse planes. At 3.0 T, the T1-relaxation times are increased compared with lower field strengths,[35] resulting in reduced tissue contrast with T1-weighted imaging; consequently, T1-weighted FLAIR images was acquired.[36] The sequence parameters were: time of repetition (TR) = 2500 ms; time of echo (TE) = 5.7 ms; inversion time = 700 ms; echo train length (ETL) = 10; bandwidth = 31.25 KHz; number of excitation (NEX) = 0.5, phase field-of-view (pFOV) = 0.7; matrix size = 160 × 128 (256 × 256 after reconstruction with zero-padding); field of view (FOV) = 22 cm; and slice thickness = 4 mm without any interslice spaces. Twenty-five phases of images were acquired, separated by either 8 s (for lower resolution of 256 × 256) or 14 s (for high resolution of 512 × 512) per phase.

The paramagnetic contrast agent, gadopentetate dimeglumine# or Gd-DTPA, was injected IV as a bolus (0.2 mmol/kg) after the first acquisition pulse. Contrast medium injection was performed by hand over approximately 3–5 s using an IV cathether in the cephalic vein.

*Hydromorphone HCl Injectable; Baxter Healthcare Corp., Deerfield, IL1.
†Versed; Roche Laboratories, Nutley, NJ.
‡Robinul; Fort Dodge Animal Health, Fort Dodge, IA.
§PropoFlo; Abbott Animal Health, North Chicago, IL.
¶IsoFlo; Abbott Animal Health.
‖General Electric Healthcare, Milwaukee, WI.
#Magnevist; Bayer Healthcare, Wayne, NJ.

After contrast medium administration, approximately 3.0 ml of 0.9% NaCl was injected to flush the catheter.

Image analysis was performed on a voxel-by-voxel basis. First, segmentation was applied using Matlab** so enhancing areas can be extracted from the background. Necrotic or edematous areas were not differentiated at this point. Next, the time course of all enhanced voxels was analyzed using the following two methods.

First, a pharmacokinetic model was used to estimate blood volume and blood vessel permeability associated with the tumor. A typical two-compartment model has been described by Tofts et al.[30] as

$$\frac{dC_t}{dt} = K^{trans}(C_p - C_t/v_e) = K^{trans}C_p - k_{ep}C_t, \quad (1)$$

where C_t and C_p are the concentration of the contrast medium in the extravascular extracellular space (e.g., leakage tissue) and plasma space, respectively. In Eq. (1), $k_{ep} = K^{trans}/v_e$, K^{trans} is the transfer constant between the plasma and the extravascular extracellular space, and v_e is the fraction volume occupied by the extravascular extracellular space. However, the concentration of contrast medium in plasma, referred to as the arterial input function (AIF) C_p is difficult to obtain or estimate. Typically the AIF is determined from blood samples[29] and represented as the sum of n decaying exponentials (usually three). In addition, the AIF can also be determined from DCE-MRI images, provided that an appropriately sized artery is included in the field of view.[37,38]

Alternatively, the signal intensity $S(t)$ obtained from a sequence of T1-weighted images changes in proportion to the contrast medium concentration C_t in the volume element of measurement, such as an area of lesion or reference region. Instead of obtaining the plasma concentration C_p in Eq. (1), an enhancement model[31] was used in this study to estimate the pharmacokinetic parameters,

$$\frac{S(t)}{S(0)} = 1 + kE_R\left(\frac{e^{-K_{ep}t} - e^{-K_{el}t}}{K_{el} - K_{ep}}\right), \quad (2)$$

where $S(t)$ is the signal intensity and $S(0)$ is the intensity at $t = 0$, and k is a dimensionless constant. The parameters E_R (rate of enhancement, min^{-1}), K_{ef} (rate of elimination, min^{-1}), and K_{ep} (rate constant, min^{-1}) of the pharmacokinetics model were estimated, based on the signal enhancement curve from the FLAIR sequence after a bolus injection (Table 1). Enhancing brain tumors with DCE-MRI and an enhancement curve from a voxel of the tumor are shown in Fig. 1.

Second, a linear approach[29,39] was chosen for evaluating the following relationship between the acquired MR signal intensity $S(t)$ and contrast medium concentration

$$C(t) : S(t) = S(0)(1 + mC(t)),$$

**The Mathworks, Natick, MA.

TABLE 1. Definitions of Heuristic Parameters in the Enhancement Model (Eq. [2]) Describing the Two-Compartment Model

Parameters	Definition	Units
E_R	Initial enhancement rate	1/min
K_{el}	Elimination rate of contrast agent	1/min
K_{ep}	Rate constant between extravascular extracellular space and blood plasma	1/min

where $S(0)$ is the signal intensity of postenhancement at $t = 0$, m is a tissue-, sequence-, and contrast medium-dependent proportional constant. This approach is valid only when $(TR \times C/T_1) \ll 1$. Consequently, signal linearity is limited to low contrast medium concentrations. In this study, trapezoidal integration was used to calculate contrast medium concentration with time after arrival of the contrast medium in the enhancing voxels of interest:

$$\text{IAUGC} = \sum_{n=0}^{N-1} \frac{(C_t(n) + C_t(n-1))(t(n) - t(n-1))}{2}, \quad (3)$$

where $C(t)$ is the tissue concentration of contrast medium at dynamic time point n, $t(n)$ is the time at point n. In Eq. (3), MR signals of the first 90 s after arrival of the contrast medium in the enhancing voxels of interest is used, a DCE-MRI measurement method suggested by the National Cancer Institute of the National Institutes of Health.[40]

All calculations, unless otherwise stated, were performed using Matlab.** Motion artifact, if present, was corrected using an MR image analysis toolbox, FSL (FMRIB Software Library, University of Oxford) software. Pharmacokinetic model fitting and the IAUGC measurement were performed on a voxel-by-voxel basis and then the parameters were averaged over the tumor volume. For model fitting of Eq. (2), the time series from each voxel was analyzed using a nonlinear least square curve fitting procedure of Matlab. For the IAUGC, the time series of the first 90 s postenhancement was used according to Eq. (3).

To study the correlation between the pharmacokinetic parameters and model-free parameter of IAUGC, Pearson's correlation was calculated between the three parameters, E_R (rate of enhancement, min^{-1}), K_{ef} (rate of elimination, min^{-1}), K_{ep} (rate constant, min^{-1}) with the IAUGC to find potential correlations between the two approaches.

To determine if any two tumors differed significantly, the two-sample Kolmogorov–Smirnov test (KS test) was used. The KS test has the advantage of making no assumption about the distribution of data. A 7×7 matrix M is obtained from a pair wise KS test among all seven tumors using each of the three kinetic parameters. Each component m_{ij} of the matrix M is a P-value. When m_{ij} is equal or close to 1 it indicates that tumor case i and j come from the same distribution. A m_{ij} equal or close to 0 indicates tumor case i and j come from different distribution.

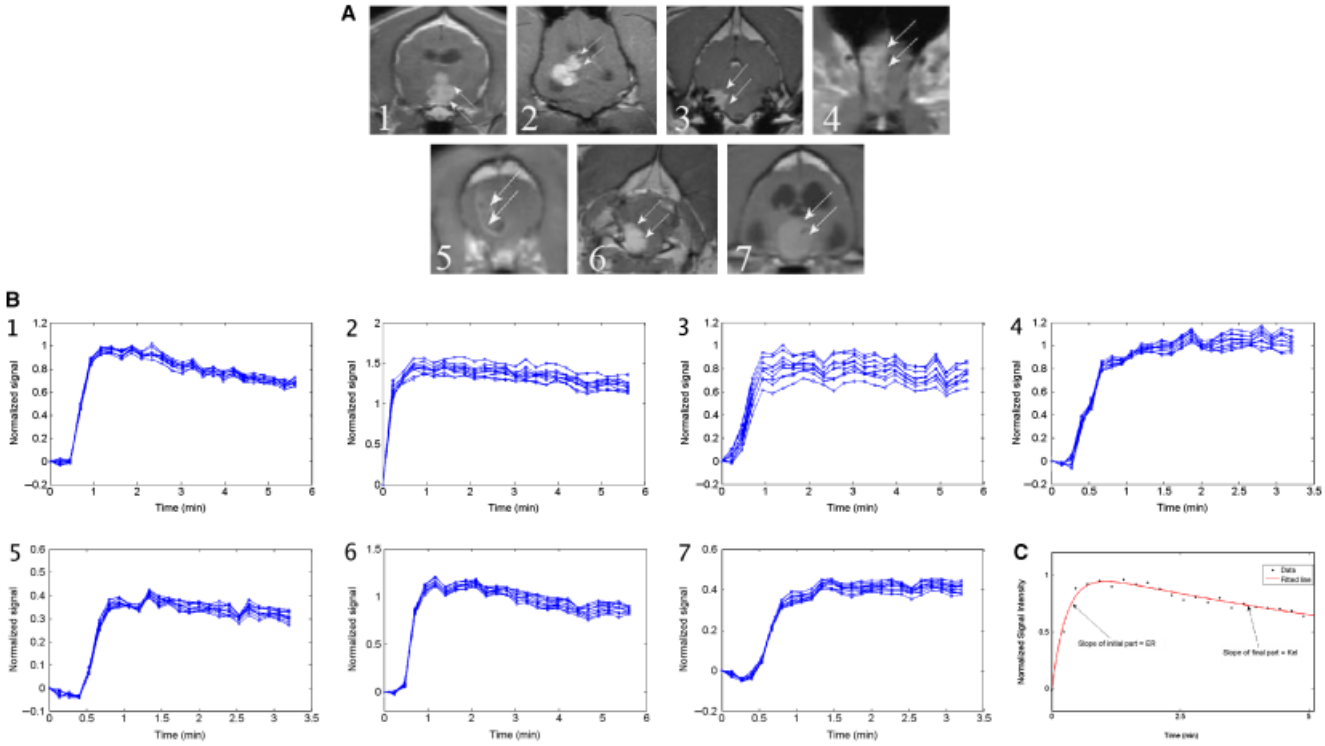

FIG. 1. (A) Enhancing tumors (indicated by arrows) for all seven brain tumor cases: adenocarcinoma (case 1), ependymoma (case 2), meningioma (case 3), meningioma (case 4), oligodendroglioma (case 5), meningioma (case 6), and macroadenoma (case 7). The T1-weighted fluid-attenuated inversion recovery sequence was used to acquire the dynamic contrast-enhanced magnetic resonance imaging data on 2D axial planes. TR/TE = 2500/5.7 ms; inversion time = 700 ms; echo train length = 10; bandwidth = 31.25 kHz; matrix size = 256 × 256 (lower resolution) or 512 × 512 (higher resolution); FOV = 22 cm; and slice thickness = 4 mm. (B) Enhancement curves of all seven cases; (C) fitting an enhancement curve from a voxel in the tumor: black dots are experimental data, with the *y*-axis indicating the normalized signal intensity and *x*-axis representing time. The red curve represents a nonlinear least square fitting result, where E_R is related to the initial enhancement rate (slope of the initial rise in the curve) and K_{el} is related to the slope of final part of the curve (elimination part).

Results

The mean and standard deviation of the three kinetic parameters, E_R (rate of enhancement, min^{-1}), K_{ef} (rate of elimination, min^{-1}), and K_{ep} (rate constant, min^{-1}), estimated for all seven tumors are listed in Table 2. The measurement of IAUGC in the initial 90 s is also reported in Table 2.

Histograms of the three pharmacokinetic parameters and model-free parameter IAUGC are presented in Fig. 2, where the rows represent tumors (from one to seven) and the columns denote the pharmacokinetic parameters (E_R, K_{ep}, and K_{el}) and model-free parameter IAUGC, respectively. All of the parameters were characterized by a unimodal distribution and have distinct features.

Pearson's correlations were calculated for the three parameters, E_R, K_{el}, and K_{ep}, with the model-free parameter IAUGC (Table 3). The IAUGC has a strong association with the rate of enhancement E_R, with r ranges from 0.4 to 0.9, but is weakly associated with K_{ep} and K_{el}.

KS test results of the kinetic parameters are shown in Table 4, for E_R, K_{el}, K_{ep}, respectively. Each matrix gives a pairwise two-sample KS test among the seven tumors, where the null hypothesis is two data sets come from

TABLE 2. Case Estimate (Mean and Standard Deviation) of Three Parameters E_R (1/min), K_{ep} (1/min), and K_{el} (1/min), and Model-Free Parameter IAUGC

Tumor	E_R	K_{ep}	K_{el}	IAUGC
Adenocarcinoma	2.07 ± 0.82	2.41 ± 1.14	0.12 ± 0.07	50.68 ± 14.36
Ependymoma	6.12 ± 1.73	5.16 ± 1.24	0.03 ± 0.01	88.02 ± 16.94
Meningioma	2.80 ± 1.21	3.36 ± 1.25	0.03 ± 0.02	60.40 ± 15.90
Meningioma	2.48 ± 1.00	3.39 ± 0.91	−0.03 ± 0.04	54.45 ± 23.73
Oligodendroglioma	1.01 ± 0.27	4.42 ± 1.53	−0.07 ± 0.04	19.36 ± 6.74
Meningioma	2.85 ± 0.29	2.18 ± 0.15	0.09 ± 0.01	75.51 ± 7.60
Macroadenoma	1.44 ± 0.20	3.32 ± 0.44	0.059 ± 0.06	28.76 ± 2.08

IAUGC, initial area under the Gd concentration curve.

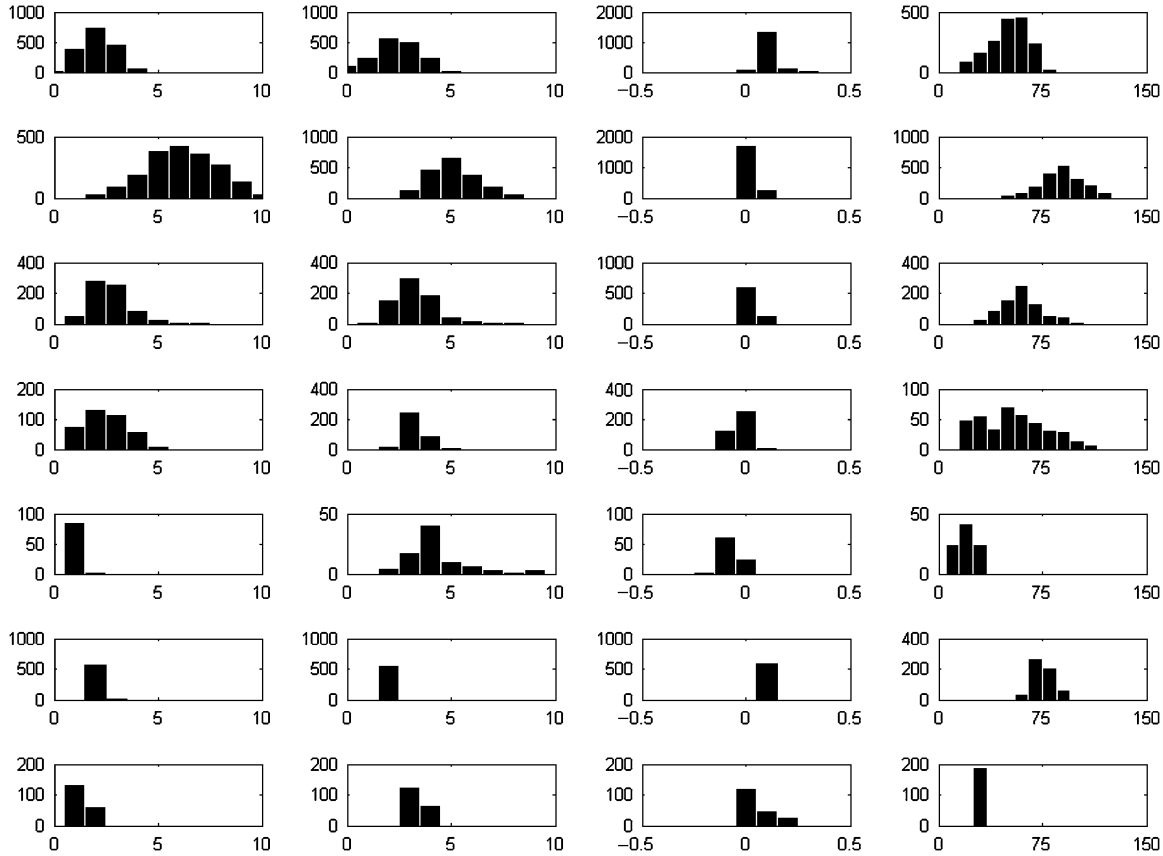

FIG. 2. Distribution histograms of the three pharmacokinetic parameters and model-free parameter initial area under the Gd concentration curve (IAUGC). The rows represent the seven cases of tumor, and the columns denote the pharmacokinetic parameters (E_R, K_{ep}, and K_{el}, all with units of 1/min) and model-free parameter IAUGC, respectively.

the same distribution. Every component in the matrix is a *P*-value, where a value of one implies that the two data sets of parameters compared have the same distribution, and a value of 0 or <0.05 means they come from different distribution. Except the diagonal components of the matrix where each tumor is compared with itself, all other components have significant differences ($P<0.05$) between any two of the seven tumors. This indicates that statistically significant differences exist between any two given parameter distributions.

TABLE 3. Case-Wise Pearson's Correlation Coefficients *r* Between the Three Parameters, E_R, K_{ep}, K_{el}, and the Model-Free Parameter IAUGC

Tumor	IAUGC and E_R	IAUGC and K_{ep}	IAUGC and K_{el}
Adenocarcinoma	0.81	0.30	−0.43
Ependymoma	0.68	0.14	0.02
Meningioma	0.66	0.15	0.42
Meningioma	0.93	−0.28	0.28
Oligodendroglioma	0.61	−0.68	−0.13
Meningioma	0.91	−0.04	−0.12
Macroadenoma	0.44	−0.03	−0.04

The IAUGC has a strong association with E_R, but is weakly associated with K_{ep} and K_{el}. IAUGC, initial area under the Gd concentration curve.

Discussion

DCE-MRI was used to investigate seven canine brain tumors. The complete tissue-specific information contained in an enhancement time series is characterized by four parameters: (1) the initial enhancement rate parameter E_R, which is proportional to the volume transfer constant in Eq. (1), K^{trans}, which also characterizes the perfusion and vascular permeability; (2) the rate constant, K_{ep}, the ratio of two physiologically fundamental parameters K^{trans} and the EES per unit volume of tissue, v_e, which approximates the rate constant of backflow from the EES to the plasma; (3) the elimination rate constant, K_{el}; and (4) the IAUGC, a measurement of the initial arrival of contrast medium in the tissue after its administration, reflecting blood flow, vascular permeability, and the fraction of interstitial space. In human studies the kinetic parameters correlate well with vascular permeability and angiogenesis within tumor tissues.[26] Further work is needed to assess whether the differences we observed between the different tumors can be confirmed. Possible pathological relevance of these parameters is that increased vascular permeability may be seen in more vascular tumors that may relate to

TABLE 4. Case-Wise Differences of the Three Parameters

Tumor	1	2	3	4	5	6	7
KS test for E_R							
1. Adenocarcinoma	1	0	0	0	0	0	0
2. Ependymoma	0	1	0	0	0	0	0
3. Meningioma	0	0	1	0	0	0	0
4. Meningioma	0	0	0	1	0	0	0
5. Oligodendroglioma	0	0	0	0	1	0	0
6. Meningioma	0	0	0	0	0	1	0
7. Macroadenoma	0	0	0	0	0	0	1
KS test for K_{el}							
1. Adenocarcinoma	1	0	0	0	0	0	0
2. Ependymoma	0	1	0	0	0	0	0
3. Meningioma	0	0	1	0	0	0	0
4. Meningioma	0	0	0	1	0	0	0
5. Oligodendroglioma	0	0	0	0	1	0	0
6. Meningioma	0	0	0	0	0	1	0
7. Macroadenoma	0	0	0	0	0	0	1
KS test for K_{ep}							
1. Adenocarcinoma	1	0	0	0	0	0	0
2. Ependymoma	0	1	0	0	0	0	0
3. Meningioma	0	0	1	0	0	0	0
4. Meningioma	0	0	0	1	0	0	0.0356
5. Oligodendroglioma	0	0	0	0	1	0	0
6. Meningioma	0	0	0	0	0	1	0
7. Macroadenoma	0	0	0	0.0356	0	0	1

Two-sample KS test were performed. Each component in the matrix is a *P*-value. A value of one implies the two data sets of parameters compared come from the same distribution, while a value of zero implies they have different distributions. KS test, Kolmogorov–Smirnov test.

more cytologicallly aggressive neoplasia. This may also be more expected in glial tumors rather than meningeal tumors based on their pathology.

A T1-FLAIR sequence was used to acquire MR data after an IV bolus injection (0.2 mmol/kg) of the paramagnetic contrast medium Gd-DTPA. Such low molecular weight contrast medium diffuses from the blood pool into the extravascular extracellular space of the brain at a rate determined by blood flow, the permeability of the blood–brain barrier, and the surface area of the perfusing vessels.[30] The contrast medium does not cross cell membranes; therefore, the volume of distribution is effectively equal to the extravascular extracellular space. On T1-weighted images, T1 relaxation time shortening caused by the contrast medium in the interstitial space is the dominant mechanism of enhancement. The early phase of contrast enhancement involves the arrival of contrast medium in the tissue of interest via the arterial supply, lasting multiple cardiac cycles. In the absence of an intact blood–brain barrier, contrast medium immediately begins to diffuse into tissue compartments with well vascularized lesions having the earliest signal increase, followed by areas of gliosis and necrosis. Over a period lasting many minutes to hours, the contrast medium diffuses back into the vasculature. Contrast medium elimination from poorly perfused tissue such as gliosis and necrosis occurs more slowly and accounts for the persistent delayed enhancement observed in malignant glial tumors.[25,26]

Simple visual analysis of enhancement seen on T1-weighted images of the brain is a valuable diagnostic tool in a number of clinical situations.[15,20,41–44] Contrast enhancement enables focal brain diseases to be visualized even when no abnormality is visible on nonenhanced images. This led to marked improvements in the sensitivity of MR imaging for detection and delineation of pathologic processes, including primary and secondary tumors and inflammation.[43,45] Unfortunately, although the presence of contrast enhancement can assist with tumor type identification in conjunction with other parameters such as tumor location, shape, and border definition, the enhancement characteristics do not correlate with tumor grade or tumor type.[15] Additionally, the sheer presence of contrast medium is not a useful objective marker for the assessment of tumor control following treatment as it can represent diverse lesions as primary tumor, tumor recurrence, gliosis, or necrosis. DCE-MRI can provide more objective criteria by which brain disease can be assessed. DCE-MRI has been used in dogs for the evaluation of the normal pituitary gland and for the evaluation of thermal coagulation of experimental tumors.[46,47]

For low contrast medium concentration, the two-compartment pharmacokinetic model is characterized by a linear relationship between signal enhancement and the contrast medium concentration for spin echo and inversion recovery sequences.[29,31] A similar enhancement model was proposed for a 3D gradient echo sequence.[33] In the pharmacokinetic model (Eq. [2]), three parameters E_R, K_{el}, and K_{ep}, were estimated. As pointed out by different groups,[29,33] E_R determines the initial enhancement rate or simply the slope of the initial wash-in period of the signal-enhancement curve, K_{el} represents the rate of elimination of the contrast agent, and K_{ep} is the rate constant between the extravascular extracellular space and plasma.

For the model-free parameter of (Eq. [3]), a linear approach was applied to represent the relationship between signal intensity $S(t)$ and contrast medium concentration $c(t)$. This approach is valid only under the condition of $(TR \times c/T_1) \ll 1$. Consequently, signal linearity is limited to low contrast medium concentrations. However, a nonlinear approach of depicting the signal intensity $S(t)$ and contrast medium concentration $c(t)$ is preferred, as the nonlinearity between $S(t)$ and $c(t)$ can represent more accurate parameter estimation in DCE-MRI studies.[48]

It was expected that the two-compartment pharmacokinetic model-based assessments of the DCE-MRI time series would have an advantage over the model-free parameter IAUGC in that the pharmacokinetic model represents the true underlying physiology of the tumor. However, the pharmacokinetic model-based parameters are generally more susceptible to the effects of noise and

fitting errors than the simpler model-free parameter, and are often assumed to be less robust.[49] On the other hand, the IAUGC might be assumed to be less variable as there is no data-fitting process involved. The relationship between IAUGC and parameters of the pharmacokinetic model was investigated used simulations of DCE-MRI data. IAUGC was shown to be related to the transfer constant K^{trans}, fractional extravascular extracellular volume v_e and fractional plasma volume v_p, and ultimately has an intractable relationship with all three. Furthermore, the range over which IAUGC is taken and the nature of the vascular (arterial) input function do not significantly affect this relationship. In the present study, we found a strong association between IAUGC and the rate of enhancement E_R, with a correlation coefficient ranging from 0.44 to 0.93; however, the association between IAUCS and K_{ep} and K_{el} was weak. However, it should be pointed out that IAUGC cannot be used as a simple surrogate for E_R despite the stronger association between IAUGC and E_R. Overall, the model-free parameter IAUGC can be complementary to the pharmacokinetic model-based parameters.

As seen in the Table 2 and Fig. 2, variation between the estimated pharmacokinetic model-based and model-free parameters can be pronounced, which makes the task of differentiation of brain tumors difficult. This was partly due to limitations of the segmentation algorithm that differentiates tumor from background. In this study, a Matlab edge detection function was used with manual override. Depending on the signal-to-noise ratio of the DCE-MRI data, and other enhancement areas in the background, segmentation results will vary from tumor to tumor. A more robust segmentation algorithm is needed.

To improve the accuracy of the estimated parameters from the pharmacokinetic models and to provide better indices for clinical diagnosis of brain tumors, one needs to understand the limitation of the models. A Bayesian Markov Chain Monte Carlo analysis could improve accuracy of the pharmacokinetic modeling.

In extracranial tumors, an association between DCE-MRI parameters and microvessel density (MVD) measurements was discovered.[50–53] This relationship has also been identified for human brain tumors, and was shown to have prognostic value.[54] More important than MVD correlations is tumor grading, and in humans there are several studies of human glioma where tumor grade was related to DCE-MRI kinetic parameters.[55–58] Also, based on MIB-1 immunohistochemistry, DCE-MRI kinetic parameters may correlate with mitotic activity of the tumor.[57] In our initial work, we determined that kinetic parameter differences of contrast enhancement may exist between various brain tumor types, even though associations with tumor vascularity or malignancy were not performed. These initial data will be helpful in designing larger prospective studies to confirm such associations.

In conclusion, we described the clinical use of DCE-MRI in dogs with brain tumors. While the study is small, it provided evidence that objective assessment of contrast enhancement may be able to assist with the differentiation of tumors.

ACKNOWLEDGMENT

The authors wish to thank Kim Mason for assistance in data acquisition and Jason Langley for assistance in image processing.

REFERENCES

1. Platt SR, Scase TJ, Adams V, et al. Vascular endothelial growth factor expression in canine intracranial meningiomas and association with patient survival. J Vet Intern Med 2006;20:663–668.

2. Dickinson PJRB, Higgins RJ, Leutenegger CM, Bollen AW, Kass PH, LeCouteur RA. Expression of receptor tyrosine kinases VEGFR-1 (FLT-1), VEGFR-2 (KDR), EGFR-1, PDGFRα and c-Met in canine primary brain tumours. Vet Comp Oncol 2006;4:132–140.

3. Koestner A, Bilzer T, Fatzer R, Schulman FY, Summers BA, Van Winkle TJ. Histological classification of tumors of the nervous system of domestic animals. In: WHO (ed): 2nd ed. Washington, DC: The Armed Forces Institute of Pathology, 1999:1–71.

4. Heidner GL, Kornegay JN, Page RL, et al. Analysis of survival in a retrospective study of 86 dogs with brain tumors. J Vet Intern Med 1991;5:219–226.

5. Courtay-Cahan C, Platt SR, De Risio L, et al. Preliminary analysis of genomic abnormalities in canine meningiomas. Vet Comp Oncol 2008;6: 182–192.

6. Thomson SA, Kennerly E, Olby N, et al. Microarray analysis of differentially expressed genes of primary tumors in the canine central nervous system. Vet Pathol 2005;42:550–558.

7. Theon AP, Lecouteur RA, Carr EA, et al. Influence of tumor cell proliferation and sex-hormone receptors on effectiveness of radiation therapy for dogs with incompletely resected meningiomas. J Am Vet Med Assoc 2000;216:701–707, 684–705.

8. Stoica G, Kim HT, Hall DG, et al. Morphology, immunohistochemistry, and genetic alterations in dog astrocytomas. Vet Pathol 2004;41: 10–19.

9. Lipsitz D, Higgins RJ, Kortz GD, et al. Glioblastoma multiforme: clinical findings, magnetic resonance imaging, and pathology in five dogs. Vet Pathol 2003;40:659–669.

10. Westworth DR, Dickinson PJ, Vernau W, et al. Choroid plexus tumors in 56 dogs (1985–2007). J Vet Intern Med 2008;22:1157–1165.

11. Patnaik AK, Kay WJ, Hurvitz AI. Intracranial meningioma: a comparative pathologic study of 28 dogs. Vet Pathol 1986;23: 369–373.

12. Montoliu P, Anor S, Vidal E, et al. Histological and immunohistochemical study of 30 cases of canine meningioma. J Comp Pathol 2006; 135:200–207.

13. Rossmeisl JH, Duncan RB, Huckle WR, et al. Expression of vascular endothelial growth factor in tumors and plasma from dogs with primary intracranial neoplasms. Am J Vet Res 2007;68:1239–1245.

14. Vandevelde M, Fankhauser R, Luginbuhl H. Immunocytochemical studies in canine neuroectodermal brain tumors. Acta Neuropathol 1985; 66:111–116.

15. Sturges BK, Dickinson PJ, Bollen AW, et al. Magnetic resonance imaging and histological classification of intracranial meningiomas in 112 dogs. J Vet Intern Med 2008;22:586–595.

16. Snyder JM, Shofer FS, Van Winkle TJ, et al. Canine intracranial primary neoplasia: 173 cases (1986–2003). J Vet Intern Med 2006;20: 669–675.

17. Kraft SL, Gavin PR, DeHaan C, et al. Retrospective review of 50 canine intracranial tumors evaluated by magnetic resonance imaging. J Vet Intern Med 1997;11:218–225.

18. Graham JP, Newell SM, Voges AK, et al. The dural tail sign in the diagnosis of meningiomas. Vet Radiol Ultrasound 1998;39:297–302.

19. Kraft SL, Gavin PR. Intracranial neoplasia. Clin Tech Small Anim Pract 1999;14:112–123.

20. Polizopoulou ZS, Koutinas AF, Souftas VD, et al. Diagnostic correlation of CT-MRI and histopathology in 10 dogs with brain neoplasms. J Vet Med A Physiol Pathol Clin Med 2004;51:226–231.

21. Cherubini GB, Mantis P, Martinez TA, et al. Utility of magnetic resonance imaging for distinguishing neoplastic from non-neoplastic brain lesions in dogs and cats. Vet Radiol Ultrasound 2005;46:384–387.

22. Engelhard HH. Progress in the diagnosis and treatment of patients with meningiomas. Part I: diagnostic imaging, preoperative embolization. Surg Neurol 2001;55:89–101.

23. Suzuki Y, Sugimoto T, Shibuya M, et al. Meningiomas: correlation between MRI characteristics and operative findings including consistency. Acta Neurochir (Wienheim) 1994;129:39–46.

24. Dickinson PJ, Sturges BK, Higgins RJ, et al. Vascular endothelial growth factor mRNA expression and peritumoral edema in canine primary central nervous system tumors. Vet Pathol 2008;45:131–139.

25. Barrett T, Brechbiel M, Bernardo M, et al. MRI of tumor angiogenesis. J Magn Reson Imaging 2007;26:235–249.

26. Padhani AR, Husband JE. Dynamic contrast-enhanced MRI studies in oncology with an emphasis on quantification, validation and human studies. Clin Radiol 2001;56:607–620.

27. Daldrup-Link H, Rydland J, Helbich T, et al. Quantification of breast tumor microvascular permeability with feruglose-enhanced MR imaging: initial phase II multicenter trial. Radiology 2003;229: 885–892.

28. Morakkabati N, Leutner C, Schmiedel A, et al. Breast MR imaging during or soon after radiation therapy. Radiology 2003;229: 893–901.

29. Tofts P. Modeling tracer kinetics in dynamic Gd-DTPA MR imaging. J Magn Reson Imaging 1997;7:91–101.

30. Tofts P, Brix G, Buckley D, et al. Estimating kinetic parameters from dynamic contrast-enhanced T(1)-weighted MRI of a diffusable tracer: standardized quantities and symbols. J Magn Reson Imaging 1999;10: 223–232.

31. Brix G, Semmler W, Port R, et al. Pharmacokinetic parameters in CNS Gd-DTPA enhanced MR imaging. J Comput Assist Tomogr 1991; 15:621–628.

32. Larsson H, Stubgaard M, Frederiksen J, et al. Quantitation of blood–brain barrier defect by magnetic resonance imaging and gadolinium-DTPA in patients with multiple sclerosis and brain tumors. Magn Reson Med 1990;16:117–131.

33. Workie D, Dardzinski B, Graham T, et al. Quantification of dynamic contrast-enhanced MR imaging of the knee in children with juvenile rheumatoid arthritis based on pharmacokinetic modeling. Magn Reson Imaging 2004;22:1201–1210.

34. Evelhoch JL. Key factors in the acquisition of contrast kinetic data for oncology. J Magn Reson Imaging 1999;10:254–259.

35. Seymour H, Koenig RDB III. Determinants of proton relaxation rates in tissue. Magn Reson Med 1984;1:437–449.

36. Winfried AW, Christiane KK. 3.0T neuroimaging: technical considerations and clinical applications. Neuroimaging Clinics North Am 2006;16:217–228.

37. Carroll TJ, Rowley HA, Haughton VM. Automatic calculation of the arterial input function for cerebral perfusion imaging with MR imaging. Radiology 2003;227:593–600.

38. Fritz-Hansen T, Rostrup E, Larsson HB, et al. Measurement of the arterial concentration of Gd-DTPA using MRI: a step toward quantitative perfusion imaging. Magn Reson Med 1996;36:225–231.

39. Hoffmann U, Brix G, Knopp M, et al. Pharmacokinetic mapping of the breast: a new method for dynamic MR mammography. Magn Reson Med 1995;33:506–514.

40. National Cancer Institute. DCE-MRI group consensus recommendations. NCI CIP MR Workshop on Translational Research in Cancer — Tumor Response. Available at http://imaging.cancer.gov/reportsandpublications/ReportsandPresentations/MagneticResonance

41. Falzone C, Rossi F, Calistri M, et al. Contrast-enhanced fluid-attenuated inversion recovery vs. contrast-enhanced spin echo T1-weighted brain imaging. Vet Radiol Ultrasound 2008;49:333–338.

42. Westworth DR, Dickinson PJ, Vernau W, et al. Choroid plexus tumors in 56 dogs (1985–2007). J Vet Intern Med 2008;22:1157–1165.

43. Mellema LM, Samii VF, Vernau KM, et al. Meningeal enhancement on magnetic resonance imaging in 15 dogs and 3 cats. Vet Radiol Ultrasound 2002;43:10–15.

44. Tidwell AS, Jones JC. Advanced imaging concepts: a pictorial glossary of CT and MRI technology. Clin Tech Small Anim Pract 1999; 14:65–111.

45. Runge VM, Muroff LR, Wells JW. Principles of contrast enhancement in the evaluation of brain diseases: an overview. J Magn Reson Imaging 1997;7:5–13.

46. Kangasniemi M, Stafford RJ, Price RE, et al. Dynamic gadolinium uptake in thermally treated canine brain tissue and experimental cerebral tumors. Invest Radiol 2003;38:102–107.

47. Graham JP, Roberts GD, Newell SM. Dynamic magnetic resonance imaging of the normal canine pituitary gland. Vet Radiol Ultrasound 2000;41:35–40.

48. Heilmann M, Kiessling F, Enderlin M, et al. Determination of pharmacokinetic parameters in DCE MRI: consequence of nonlinearity between contrast agent concentration and signal intensity. Invest Radiol 2006;41:536–543.

49. Roberts C, Issa B, Stone A, et al. Comparative study into the robustness of compartmental modeling and model-free analysis in DCE-MRI studies. J Magn Reson Imaging 2006;23:554–563.

50. Buadu LD, Murakami J, Murayama S, et al. Breast lesions: correlation of contrast medium enhancement patterns on MR images with histopathologic findings and tumor angiogenesis. Radiology 1996;200:639–649.

51. Buckley DL, Drew PJ, Mussurakis S, et al. Microvessel density of invasive breast cancer assessed by dynamic Gd-DTPA enhanced MRI. J Magn Reson Imaging 1997;7:461–464.

52. Hawighorst H, Knapstein PG, Weikel W, et al. Angiogenesis of uterine cervical carcinoma: characterization by pharmacokinetic magnetic resonance parameters and histological microvessel density with correlation to lymphatic involvement. Cancer Res 1997;57:4777–4786.

53. Stomper PC, Winston JS, Herman S, et al. Angiogenesis and dynamic MR imaging gadolinium enhancement of malignant and benign breast lesions. Breast Cancer Res Treat 1997;45:39–46.

54. Tynninen O, Aronen HJ, Ruhala M, et al. MRI enhancement and microvascular density in gliomas. Correlation with tumor cell proliferation. Invest Radiol 1999;34:427–434.

55. Ludemann L, Hamm B, Zimmer C. Pharmacokinetic analysis of glioma compartments with dynamic Gd-DTPA-enhanced magnetic resonance imaging. Magn Reson Imaging 2000;18:1201–1214.

56. Ludemann L, Grieger W, Wurm R, et al. Comparison of dynamic contrast-enhanced MRI with WHO tumor grading for gliomas. Eur Radiol 2001;11:1231–1241.

57. Roberts HC, Roberts TP, Bollen AW, et al. Correlation of microvascular permeability derived from dynamic contrast-enhanced MR imaging with histologic grade and tumor labeling index: a study in human brain tumors. Acad Radiol 2001;8:384–391.

58. Roberts HC, Roberts TP, Brasch RC, et al. Quantitative measurement of microvascular permeability in human brain tumors achieved using dynamic contrast-enhanced MR imaging: correlation with histologic grade. Am J Neuroradiol 2000;21:891–899.